Mechanism of ginsenoside Rb_3 against OGD/R damage based on metabonomic and PCR array analyses

FUHUI LI[1*], JIE TAO[2*], MINGMIN ZHOU[1], XINGZHI YU[2], TIAN XIAO[2], CHAOLIANG WANG[1] and XIAOHUA DUAN[2]

[1]College of Notoginseng Medicine, Wenshan University, Wenshan, Yunnan 663099, P.R. China; [2]Yunnan Key Laboratory of Dai and Yi Medicines, Yunnan University of Chinese Medicine, Kunming, Yunnan 650500, P.R. China

Received April 14, 2024; Accepted September 4, 2024

DOI: 10.3892/br.2024.1875

Abstract. In order to study the mechanisms of ginsenoside Rb_3 (G-Rb_3) against oxygen-glucose deprivation/reoxygenation (OGD/R) injury in HT22 cells based on metabolomics and PCR array, HT22 cells were randomly divided into control group, model group, G-Rb_3 high-dose group (10 μmol/l) and G-Rb_3 low-dose group (5 μmol/l). Except for the control group, which was left untreated, the remaining groups were incubated with 10 mmol/l $Na_2S_2O_4$ in sugar-free DMEM medium for 2 h and then replaced with serum-free high-sugar DMEM medium for 2 h in order to replicate *in vitro* OGD/R model. Trypan blue staining was used to detect the cell viability; flow cytometry was used to detect apoptosis; western blotting was used to detect the protein expression levels of Bax, Bcl-2 and caspase-3. The metabolomics were used to analyze the differential metabolites of G-Rb_3 affecting OGD/R in order to find the relevant metabolic pathways. PCR array assay was performed to identify the expression of the differential genes. G-Rb_3 could inhibit HT22 apoptosis according to the result of cell morphology, trypan blue staining and flow cytometry. The levels of Bax and caspase-3 protein expression were decreased, whereas the level of Bcl-2 protein expression was increased after the treatment of G-Rb_3. Metabolomics results showed that a total of 31 differential metabolites between OGD/R group and G-Rb_3 group, such as guanosine level, was downregulated, the levels of enalaprilat and sorbitol were upregulated, affecting ABC transporters, galactose metabolism, citrate cycle and other related metabolic pathways; according to the result of PCR array, it was observed that G-Rb_3 significantly downregulated *Trp63*, *Trp73*, *Dapk1*, *Casp14* and *Cd70* pro-apoptotic genes. In conclusion, G-Rb_3 has a significant protective effect on the OGD/R model simulated *in vitro*, and the mechanism may be related to the inhibition of apoptosis by affecting metabolites.

Correspondence to: Professor Chaoliang Wang, College of Notoginseng Medicine, Wenshan University, 66 Xuefu Road, Wenshan, Yunnan 663099, P.R. China
E-mail: 1010816954@qq.com

Professor Xiaohua Duan, Yunnan Key Laboratory of Dai and Yi Medicines, Yunnan University of Chinese Medicine, 1076 Yuhua Road, Kunming, Yunnan 650500, P.R. China
E-mail: 1047896527@qq.com

*Contributed equally

Key words: ginsenoside Rb_3, oxygen glucose deprivation/reoxygenation, metabolomics, PCR array, apoptosis

Introduction

Stroke, which is the leading cause of death in China, mainly comprises cerebral hemorrhage and cerebral infarction, of which cerebral ischemia accounts for nearly 80% of stroke cases (1,2). According to survey results, stroke has become the second leading cause of death worldwide, with high rates of incidence, recurrence and high disability, especially among the elderly (3,4). Thrombolytic and neuroprotective therapies are the main clinical treatments of this disease; however, in cases of cerebral ischemia, thrombolysis and reperfusion can cause secondary damage to the brain, leading to death and disability (5-9). This undoubtedly brings economic pressure and physical and emotional pain to the families of patients. Therefore, there is an urgent need to find effective drugs for the treatment of stroke.

Traditional Chinese medicine has unique advantages and roles in the treatment of diseases. *Panax notoginseng* (Burk.) F.H. Chen is a geo-authentic Chinese medicinal material from Wenshan, Yunnan, which is used as a medicine with dried roots and rhizomes. Although there is high annual production of *Panax notoginseng* stems and leaves, the utilisation rate of the 226 saponin constituents is extremely low. The most abundant of these saponins is ginsenoside Rb_3 (G-Rb_3; $C_{53}H_{90}O_{22}$). A large amount of resource waste could be reduced by full utilization of G-Rb_3. It has been shown to have a variety of biological activities, including cardiovascular protection and brain protection (10). Liu *et al* (11) found that G-Rb_3 inhibits apoptosis and protects against myocardial ischemic-reperfusion. Ginsenosides protect against the damage brought about by oxygen-glucose deprivation/reoxygenation (OGD/R) in hippocampal neuron HT22 cells through an anti-oxidative stress mechanism (12). These findings showed that G-Rb_3 has great potential in the treatment of stroke; thus, in the present study it was aimed to define more clearly the mechanism by

which G-Rb_3 protects against cerebral ischemic-reperfusion injury (CIRI). The present study aimed to use a HT22 cell-based replica of the OGD/R model, combined with metabolomics and PCR array analyses, to determine whether G-Rb_3 ameliorates OGD/R injury through inhibition of cell apoptosis.

Liquid chromatography (LC)-mass spectrometry (MS) has been proved to be a powerful and reliable analytical method with high sensitivity and structural separation ability (13,14). The occurrence of CIRI leads to alterations in systemic metabolites, which cause a series of complex cascade reactions that ultimately lead to apoptosis (15,16). Metabolomics analysis can be used to the biological functions and metabolic pathways of metabolites *in vivo* (17,18). Therefore, untargeted metabolomics were also used to conduct an in-depth exploration of the changes in metabolite levels related to the actions of G-Rb_3 against OGD/R injury.

Materials and methods

Cell culture and drug delivery. HT22 cells derived from mouse hippocampal neuronal cell line (cat. no. CC-Y2137; Shanghai Enzyme Research Biotechnology Co., Ltd.) were utilized. High sugar medium DMEM (cat. no. 01-043-1A; Biological Industries) with 1% penicillin-streptomycin liquid (cat. no. 03-031-5B; Biological Industries) and 10% fetal bovine serum (cat. no. 504090618; Shanghai Yeasen Biotechnology Co., Ltd.) were used for cell culture at 37˚C with 5% CO_2 in a HF90 incubator (Shanghai Lishen Scientific Equipment Co., Ltd.). When the cells proliferated to the logarithmic growth period, they were transferred into 6-well plates at a concentration of $1x10^5$/ml for the subsequent experiments. G-Rb_3 (cat. no. CCPE900218; Henan Wanjia Standard Material R&D Center Co., Ltd.; https://cdn.bzwzzx.com/product/search.html?keywords=G-Rb3&pageindex=1; purity ≥99.86%) was dissolved in phosphate-buffered saline to a mother liquor concentration of 1 mmol/l. The cells were randomly divided into 4 groups: Control group, OGD/R group, G-Rb_3 high dose group (10 μmol/l) and G-Rb_3 low dose group (5 μmol/l). Since relevant cell safety experiments were already conducted in the previous study, it was found that the effective concentrations of G-Rb_3 to improve OGD/R were 2.5, 5 and 10 μmol/l (12); For the present study, it was observed that the most effective drug concentrations were 5 and 10 μmol/l and were therefore selected for the experiments.

OGD/R model. $Na_2S_2O_4$ is an effective oxygen scavenger without harming the cells, thus $Na_2S_2O_4$ (cat. no. S817915; Shanghai Macklin Biochemical Co., Ltd.) was chosen to simulate the OGD/R model in this experiment. When the cell density increased to 80-90%, except for the control group which was left untreated, the remaining groups were incubated with 10 mmol/l $Na_2S_2O_4$ in sugar-free DMEM (cat. no. 01-042-1A; Biological Industries) at 37˚C for 2 h and then replaced with serum-free high-sugar DMEM at 37˚C for 2 h in order to replicate the *in vitro* OGD/R model. Meanwhile, in the G-Rb_3 group, the drug started being added 24 h before modelling, and continued until the end of re-glycation and reoxygenation.

Trypan blue staining for cell viability measurement. HT22 cells were used to inoculate 6-well plates at a uniform inoculum density of $1x10^5$/ml (2 ml cell suspension per well). When cells proliferated to logarithmic growth phase, a total of 1 ml EDTA-free trypsin (cat. no. 15050-065; Thermo Fisher Scientific, Inc.) was added to each well at 37˚C for 1 min, followed by the addition of trypan blue (cat. no. G1019; Wuhan Servicebio Technology Co., Ltd.), which was mixed with the cell suspension at a ratio of 1:9 and was then left to stand at room temperature for 2 min. A 20 μl aliquot of the cell suspension was aspirated to a hemocytometer for observation under an inverted microscope (DMI1; Leica Microsystems Ltd.). In total, four large squares in the field of vision of the hemocytometer were selected for counting cells. Subsequently, the cell viability was calculated.

Flow cytometry to detect apoptosis. HT22 cells were used to inoculate 6-well plates at a uniform inoculum density of $1x10^5$/ml (2 ml cell suspension per well). The cells were digested with 1 ml of EDTA-free trypsin at 37˚C for 1 min and were subsequently collected. Annexin V-AbFluor™ 488/PI apoptosis detection kit (cat. no. KTA0002; Abbkine Scientific Co., Ltd.) was utilized. The cells were first resuspended in 100 μl AnnexinV Binding Buffer diluted in deionized water to which, 5 μl of AnnexinV-AbFluor™488 was added, and then incubated on ice for 15 min. A total of 2 μl propidium iodide dye was pre-added. Detected was performed by flow cytometry (FACSCelesta; BD Biosciences) within 30 min. BD FACSDiva™ software (v8.0.1.1;) was used to analyze data.

Western blotting (WB) detection of protein expression. The HT22 cells of each group in the logarithmic growth phase were collected and cultured in 6-well plates at a density of $6.5x10^5$/ml for 24 h. The cells were lysed on the ice with RIPA lysis buffer (cat. no. P0013C; Beyotime Institute of Biotechnology). The supernatant was centrifuged at 12,000 x g at 4˚C for 5 min. Determination of protein concentration by BCA method (cat. no. P0010; Beyotime Institute of Biotechnology). According to the molecular weight, 10% separation gel and 5% compression gel were prepared, 20 μg protein samples were added to each lane, and separated by SDS-PAGE electrophoresis for 30 min; the electrophoresis was terminated when the desired target band reached the appropriate position. The cut PVDF membrane (0.45 μm; cat. no. IPFL85R; MilliporeSigma) was soaked in methanol for 1 min. After the transfer, the membrane was blocked with 5% skim milk (cat. no. P0216; Beyotime Institute of Biotechnology) powder for 1 h at room temperature. Subsequently, the membranes were incubated at 4˚C overnight with the following primary antibodies: Bax (1:2,000; cat. no. 50599-2-Ig; Proteintech Group, Inc.), Bcl-2 (1:1,000; cat. no. sc-7382; Santa Cruz Biotechnology, Inc.), caspase-3 (1:1,000; cat. no. 9662; Cell Signaling Technology, Inc.) and β-actin (1:1,000; cat. no. ab8226; Abcam). Then, the membranes were incubated for 1 h at room temperature with the following secondary antibodies: Goat anti-rabbit IgG (1:10,000; cat. no. ab6721; Abcam) and rabbit anti-mouse IgG (1:10,000; cat. no. ab6728; Abcam). The aforementioned membrane washing procedure was repeated. Next, the luminescent reagent liquid A and liquid B were mixed in equal volume and were applied in the membrane. After 5 min, the

protein bands were detected with Tanon-6600 luminescence imaging workstation (Shanghai Tianneng Life Science Co., Ltd.). Protein expression was analyzed by using the ImageJ v2 software (National Institutes of Health) to analyze the optical density values.

Metabolomics sample collection. HT22 cells were inoculated into 6-well plates at a concentration of $1x10^5$/ml. The cells were divided into an OGD/R group and a G-Rb_3 group, using one sample per two wells, with a total of six samples collected for analysis. Glass beads (cat. no. G8772; Shanghai Lianshuo Biotechnology Co., Ltd.) and 1,000 μl acetonitrile (cat. no. AS1121; Shanghai Yaokan Chemical Industry Co., Ltd.) were added, and the mixture was vortexed for 30 sec and then ground for 2 min at 60 Hz in a tissue grinder. The mixture was transferred to a centrifuge tube, spun at 14,000 x g for 10 min at 4˚C, the supernatant was isolated, and 300 μl of a 2-chlorophenylalanine (4 ppm) solution were accurately prepared using acetonitrile with 0.1% formic acid (cat. no. 28905; Thermo Fisher Scientific, Inc.) (1:9, v/v). The solution was used to re-dissolve the samples. The supernatant was filtered through a 0.22 μm membrane and was subsequently added to the detection vials for LC-MS analysis.

LC/MS conditions. Chromatographic conditions: Waters ACQUITY (Waters Corporation) and ACQUITY UPLC® HSS T3 (2.1x150 mm, 1.8 μm) (Waters Corporation) column were used with a flow rate of 0.25 ml/min at 40˚C. The injection volume was 2 μl. The mobile phases were: 0.1% formic acid in acetonitrile (B1) and 0.1% formic acid in water (A1) in positive ion mode, and the gradient elution program was as follows: 0-1 min, 2% B1; 1-9 min, 2-50% B1; 9-12 min, 50-98% B1; 12-13.5 min, 98% B1; 13.5-14 min, 98-2% B1; 14-12 min, 98-2% B1; 14-20 min, 2% B1. In negative ion mode, the mobile phases were acetonitrile (B2) and ammonium formate water (A2), and the gradient elution procedures were as follows: 0-1 min, 2% B2; 1-9 min, 2-50% B2; 9-12 min, 50-98% B2; 12-13.5 min, 98% B2; 13.5-14 min, 98-2% B2; 14-17 min, 2% B2.

MS conditions. A Thermo Q Exactive MS detector (Thermo Fisher Scientific, Inc.) with an electrospray ioniation source was used to collect data separately in positive and negative ion modes, the settings were as following: Positive ion spray voltage, 3.50 kV; negative ion spray voltage, -2.50 kV; sheath gas, 30 arbs; auxiliary gas, 10 arbs and capillary temperature, 325˚C. The primary full scan was performed at a resolution of 70,000 m/z, with a primary ion scanning range of 100-1,000 m/z. Higher-energy collisional dissociation was used for the secondary cleavage, with a collision energy of 30 eV and a secondary resolution of 17,500 m/z. The first 10 ions of the acquired signal were fragmented, with dynamic exclusion used to remove unnecessary tandem MS information.

Metabolic data processing and analysis. The raw files were converted to mzXML file format using MSConvert in the ProteoWizard package (v3.0.8789), with parameters set to 'bw=2', 'ppm=15', 'peakwidth=c' (parameters, 5,30), 'mzwid=0.015','mzdiff=0.01' and 'method=centWave' (19-21). After obtaining the quantitative list of substances, the following databases: HMDB (22), massbank (23), LipidMaps (24), mzcloud (25) and Kyoto Encyclopedia of Genes and Genomes (KEGG) (26) were used to identify the substances, followed by data rectification. The quality control samples with relative standard deviation >30% of the substances were removed. The R language Ropls package (v1.15.0; Autodesx) was used to perform principal component analysis (PCA), partial least-square discriminant analysis (PLS-DA). The sample data were analyzed by orthogonal partial least-square discriminant analysis (OPLS-DA) to reduce dimensions. The final screening was performed via calculating the P-value and variable projection importance (VIP) value, and metabolite molecules were considered statistically significant when the P-value was <0.05 and the VIP value was >1. Pathway analysis was mainly carried out by MetaboAnalyst software (v6.0) developed by Xia-lab of McGill University in Canada, which is used for enrichment analysis of differential metabolites obtained from screening, and for browsing differential metabolites by using pathway maps in KEGG Mapper tool (27).

Apoptosis PCR array. Firstly, according to the RNA extraction kit (cat. no. DP430; Tiangen Biotech Co., Ltd.), the RNA of OGD/R group and G-Rb_3 group was extracted, its concentration and purity were detected by a spectrophotometer and it was subsequently reversed into cDNA. The substance was diluted and mixed to a total volume of 100 μl, and was then placed on ice. According to the PCR array kit for detection of gene expression. (cat. no. wc-mRNA0263-M; Shanghai WcGene Technology Co., Ltd.; www.wcgene.cn) plates were centrifuged at 100 x g for 20 sec before use and the sealing membrane was carefully torn off at the end of centrifugation. A total of 920 μl of cDNA were prepared and mixed the components are revealed in Table I, then add the prepared mixed sample into a 96-well plate (9 μl per well), the plate was then sealed with a transparent sealing membrane, centrifuged at 100 x g for 20 sec and was finally assessed on the PCR instrument (Veriti™ 96-Well Fast Thermal Cycler; Thermo Fisher Scientific, Inc.). The reaction system was set at 10 μl, and the conditions are shown in Table II. The real time PCR reaction was started on the machine, and the results were exported for data analysis. The PCR primer sequences were not provided by the company, although the primer sequences of the differential genes are included in Table SI.

Statistical analysis. Data are expressed as the mean ± standard deviation (SD) (n=6). Data were statistically analyzed using GraphPad Prism 8.0 software (Dotmatics) and were normally distributed. If the variances were equal, Bonferroni's multiple comparison test was performed using one-way analysis of variance (ANOVA). If the conflicts were not equal, Dunnett's multiple comparison test was used in Welch's ANOVA test. P<0.05 was considered to indicate a statistically significant difference.

Results

Trypan blue staining and flow cytometry. The cell morphology after G-Rb_3 intervention indicated that G-Rb_3 effectively improved OGD/R injury (Fig. 1A). The results of trypan blue staining showed that cell viability was significantly higher in

Table I. Formulation of cDNA and components.

Components	Volume (9 μl per well in 96-well plates)
WCGENE® mRNA qPCR mix (2x)	510 μl
cDNA sample	100 μl
RNase-free ddH_2O	310 μl
Total volume	920 μl

Table II. PCR reaction conditions.

Cycle		Temperature	Time	Remarks
Pre-denaturation	1	95˚C	30 sec	-
Denaturation	40	95˚C	5 sec	-
Annealing extension	40	60˚C	30 sec	Open fluorescence acquisition channel

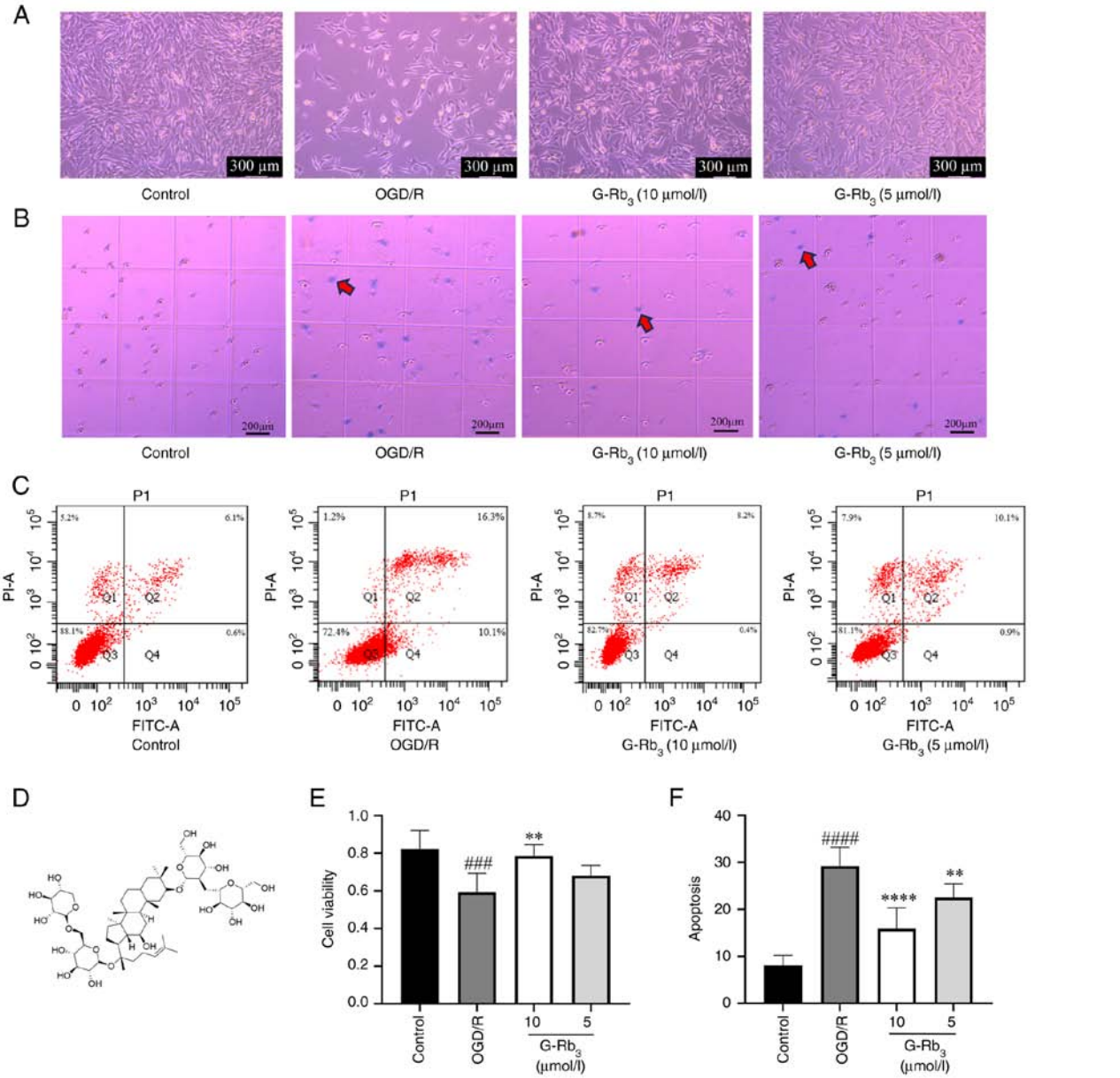

Figure 1. Effect of G-Rb_3 on OGD/R-induced HT22 cell morphology and apoptosis. (A) Morphology of HT22 cells in each group. (B) Trypan blue staining. Blue color represents apoptotic cells as indicated by red arrows in the figure, and unstained cells are normal cells. (C) Detection of apoptosis by flow cytometry. Each point in the figure represents a cell, the X-axis and Y-axis represent the fluorescence intensity of the cells in the two channels of FITC and PI, the upper left quadrant represents the cell debris, which are the mechanically damaged cells, the lower left quadrant represents the normal cells, the upper right quadrant represents the late apoptotic and necrotic cells, and the lower right quadrant represents the cells with early apoptosis. The sum of the early apoptotic and late apoptotic cells is the total number of each group of HT22 cells. The sum of early apoptotic cells and late apoptotic cells is the number of apoptotic cells in each group. (D) Chemical structure of G-Rb_3. (E) Statistics of cell survival rate by trypan blue staining. $^{###}$P=0.0003 and Q=0.0006 vs. control group; **P=0.0016 and Q=0.0016 vs. OGD/R group. (F) Statistical graph of total apoptosis rate in each group. $^{####}$P<0.0001 vs. control group; **P=0.0086 and Q=0.0086, ****P<0.0001 vs. OGD/R group. Statistical results were all analyzed by one-way ordinary ANOVA (n=6). G-Rb_3, ginsenoside Rb_3OGD/R, oxygen-glucose deprivation/reoxygenation.

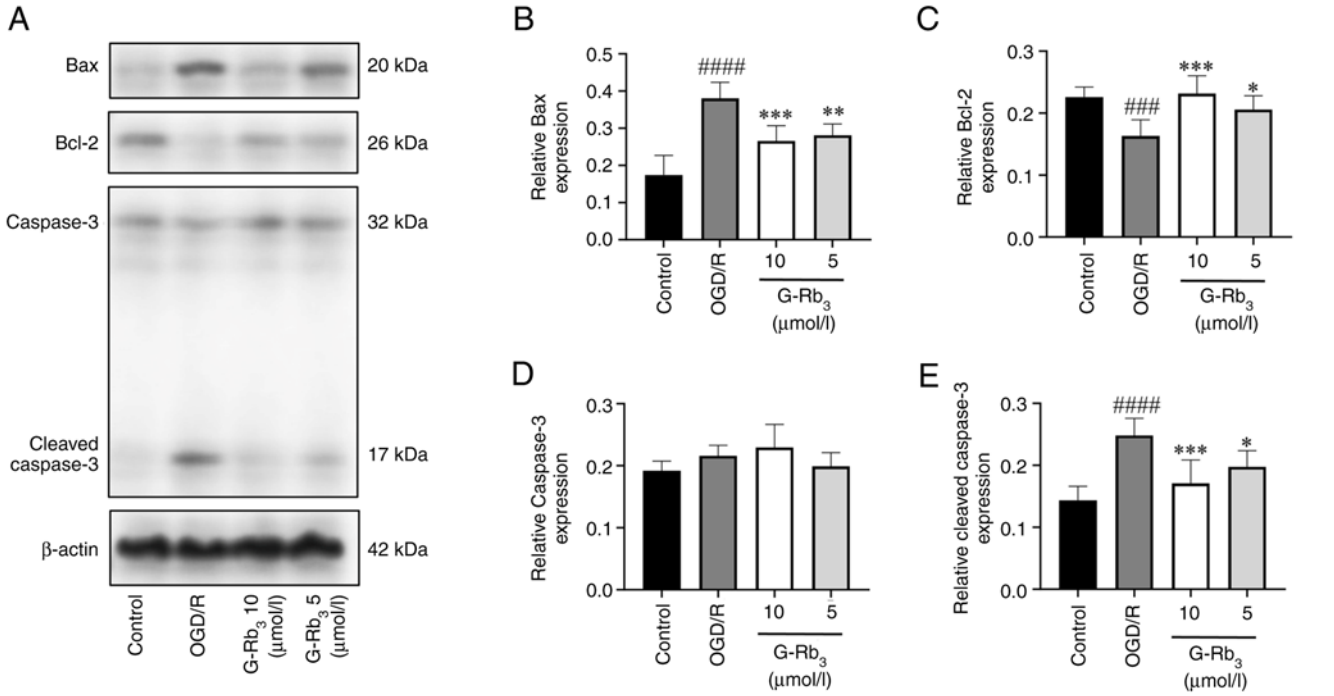

Figure 2. Western blot analysis of related protein expression. (A) Bax, Bcl-2, caspase-3 and cleaved caspase-3 protein expression are illustrated. (B) Bax protein expression statistic graph. Compared with the control group, the OGD/R group had a significant difference ($^{####}$P<0.0001) with upregulated expression, compared with the OGD/R group, and downregulated expression in the G-Rb_3 group (***P=0.0004 and Q=0.0008; **P=0.0019 and Q=0.0019). (C) Statistical graph of Bcl-2 protein expression, which was downregulated in the OGD/R group compared with the control group ($^{###}$P=0.0005 and Q=0.0015) and upregulated in the G-Rb_3 group compared with the OGD/R group with significant differences (***P=0.0002 and Q=0.0003; *P=0.0144 and Q=0.0144). (D) Caspase-3 protein expression statistics were not significantly different between the model group and the G-Rb_3 group. (E) Cleaved caspase-3 protein expression statistics had significant difference and upregulated expression in the OGD/R group compared with the control group ($^{####}$P<0.0001), downregulated expression in the G-Rb_3 group compared with the OGD/R group, and significant difference (***P=0.0005 and Q=0.001; *P=0.0185 and Q=0.185). G-Rb_3, ginsenoside Rb_3; OGD/R, oxygen-glucose deprivation/reoxygenation; kDa, kilodalton.

the drug treatment group than the model group (P<0.001), at a drug concentration of 10 μmol/l, indicating that G-Rb_3 effectively improved the survival rate of HT22 cells in the OGD/R model (Fig. 1B and E). Similarly, the apoptosis rate showed that G-Rb_3 effectively inhibited apoptosis (Fig. 1C and F). When the dose of G-Rb_3 reached 10 μmol/l, there was significant difference compared with the model group (P<0.0001). The chemical structural formula of G-Rb_3 is illustrated in Fig. 1D.

WB assay results. Protein expression levels of Bax, Bcl-2, caspase-3 and cleaved caspase-3 are shown in Fig. 2A. There was no significant difference in the expression of caspase-3 protein compared with either the control or model groups (Fig. 2D). The OGD/R group showed increased levels of Bax and cleaved caspase-3 protein expression (Fig. 2B and E), and decreased levels of Bcl-2 protein expression (Fig. 2C), compared with the control group. The levels of Bax and cleaved caspase-3 protein expression were decreased (Fig. 2B and E) and the levels of Bcl-2 protein expression were increased, compared with the G-Rb_3 group (Fig. 2C). The original blots of Fig. 2 are shown in Fig. S1.

Feasibility evaluation of metabolomics experimental data. The screening methods for differential metabolites mainly include PCA, PLS-DA and OPLS-DA. PCA is an unsupervised discriminant analysis method, which reveals clustering of the samples within the groups and dispersion of the samples between the groups. The results were reliable (Fig. 3A and B). The advantage of PLS-DA over PCA is that it is a supervised discriminant analysis method, in which the samples have to be specified and grouped, and the separation of groups was improved compared with the PCA analysis (Fig. 3C and D). The OPLS-DA is based on PLS-DA, with orthogonal transformation correction, which improves the model's resolving ability and validity. The samples were further resolved with OPLS-DA analysis to characterize the true differences between groups and identify biomarkers from them. In both positive and negative ion modes, intra-group sample clustering and inter-group sample dispersion could be observed in the OGD/R group and the G-Rb_3 group (Fig. 3E and F), suggesting that the results can be used for further analysis.

Screening for differential metabolites. In this method, P-value <0.05 and VIP value >1 were used to screen for differential metabolites between groups, and a total of 31 metabolites showed significant differences (Table III). In total, 12 metabolites were upregulated: 3-indoleacetonitrile, 4-pyridoxic acid, enalaprilat, (R) 2,3-dihydroxy-3-methylvalerate, sorbitol, yohimbine, 4-fumarylacetoacetate; pimelic acid, oleamide, dihydrouracil, linoleic acid and cis-4-hydroxy-D-proline. In addition, 19 metabolites were downregulated: geranyl diphosphate, cis-aconitate acid, D-arabitol, D-lyxose, D-galactose; alpha-D-glucose, adipic acid, isocitric acid, 6-phosphogluconic acid, 3-hydroxymethylglutaric acid, linoleic acid, thiamine, aminoethylphosphate, L-glutamate-gamma-semialdehyde, geranyl diphosphate, procollagen 5-hydroxy-L-lysine,

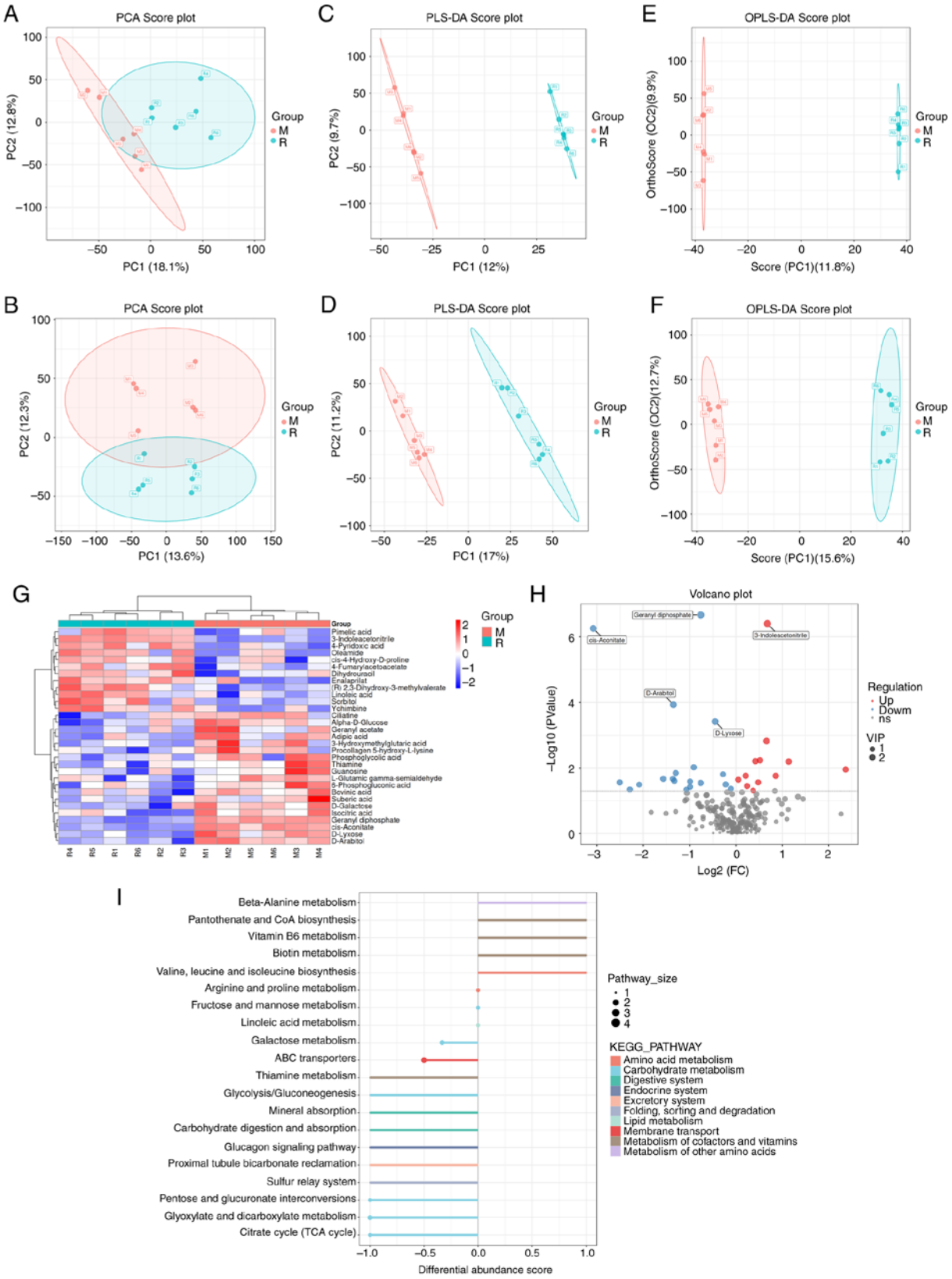

Figure 3. Detection of metabolomics data and differential metabolite screening. (A and B) PCA scores plots. Arranged in order to positive and negative ions. (C and D) PLS-DA score plots. The samples were specified and grouped in positive and negative ion order using PLS-DA to eliminate random errors unrelated to the purpose of the study. (E and F) OPLS-DA scores plots. The more clustered the samples within the group and the more dispersed the samples between the groups, the more reliable the results. (G) Clustering heat map of 31 differential metabolites. Red color means higher expression, blue color means lower expression, the top clustering line is the clustering line of OGD/R group and G-Rb_3 group, the left side is the clustering line of metabolites, and the expression of metabolites can be clearly observed on the right side. (H) Differential metabolite volcano plot. Red dots represent upregulated differential metabolites, blue dots represent downregulated differential metabolites. (I) Differential metabolite enrichment analysis score plot. Horizontal coordinate differential abundance score is the total number of upregulated metabolites-total number of downregulated metabolites/total number of metabolites. Vertical coordinate is the pathway, and the size of the dot represents the number of enriched differential metabolites in the pathway. M, Model group; R, G-Rb_3 group; PCA, principal component analysis; PLS-DA, partial least-square discriminant analysis; OPLS-DA, PLS-DA.

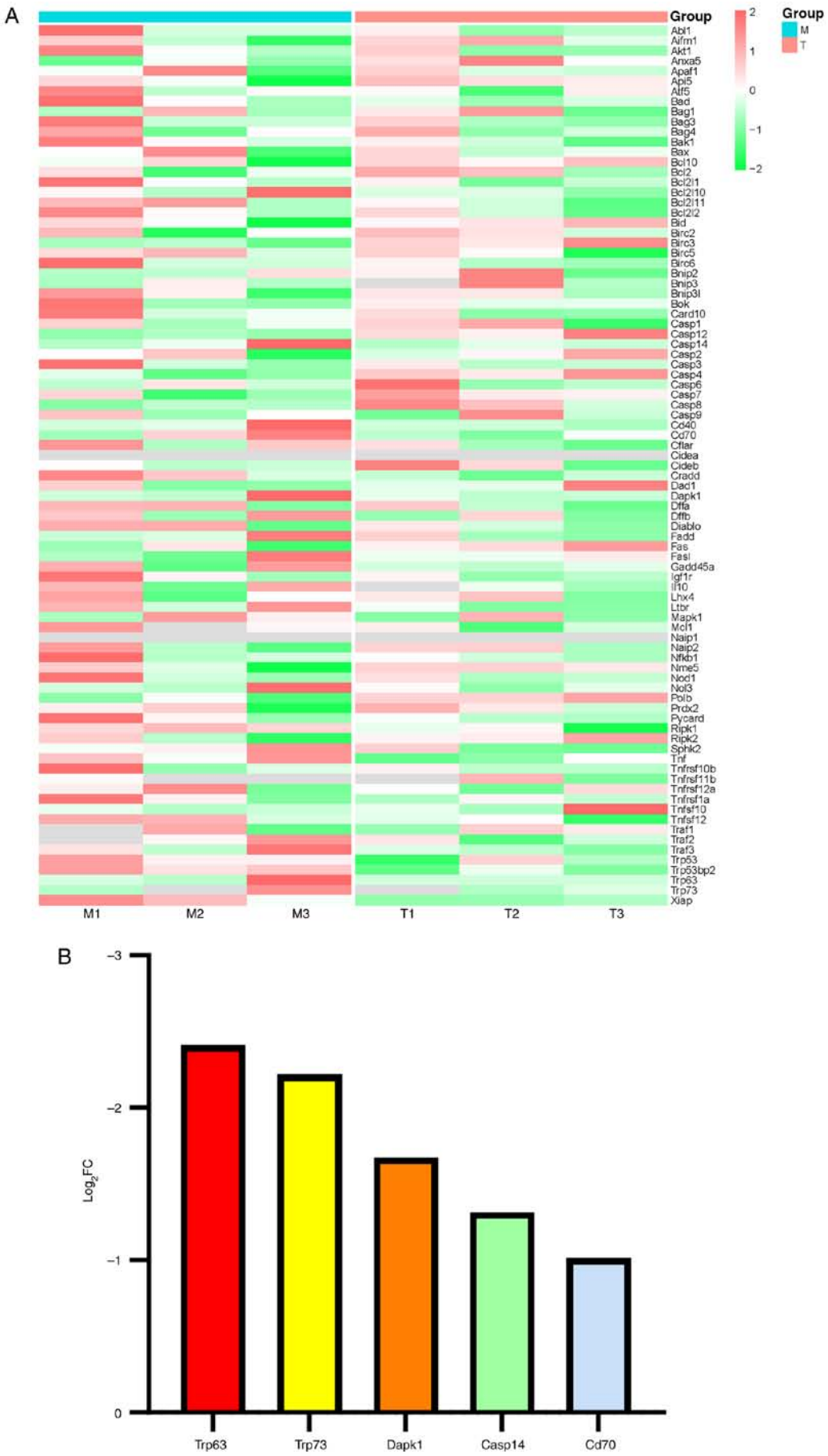

Figure 4. PCR Array. (A) PCR Array clustering heat map. Red color means higher gene expression level and green color means lower gene expression level. The right column represents gene expression status. (B) Differential gene histogram. Screening obtained a total of 5 differential genes that were downregulated, each bar representing a differential gene.

Table III. Differential metabolite statistics.

Group	Total number of metabolites	Upregulated	Downregulated	Total number of differential metabolites
RVSM	291	12	19	31

M, Model group; R, G-Rb_3 group.

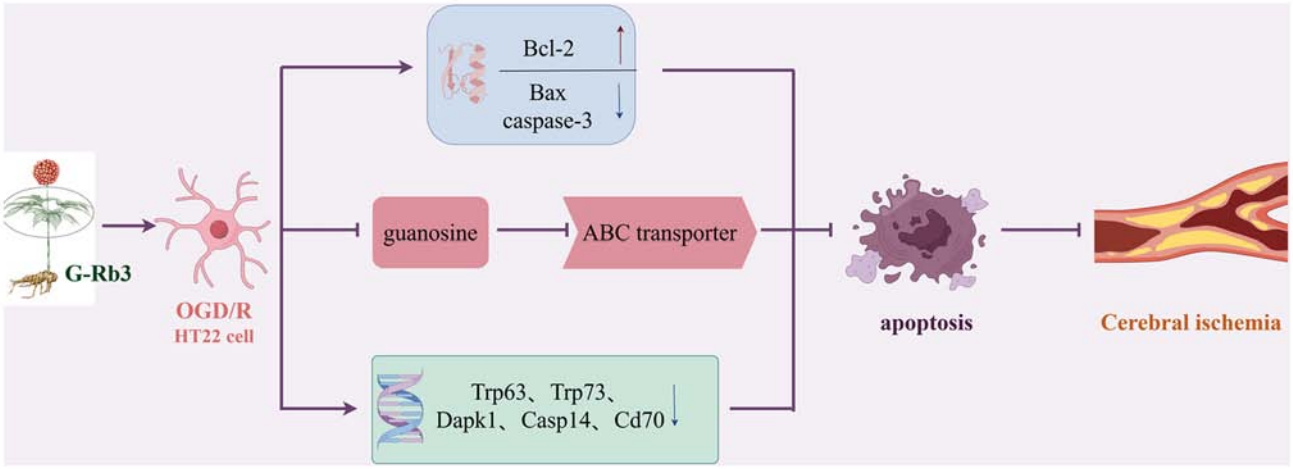

Figure 5. Summary diagram of the protective mechanism of G-Rb_3 against OGD/R-induced HT22 cells. G-Rb3 was first found to inhibit apoptosis by regulating the balance of apoptotic protein Bax/Bcl-2, then regulating the expression of guanosine, and finally verified by PCR array. Combining the aforementioned results, it was hypothesized that G-Rb3 can protect HT22 cells from OGD/R-induced damage by inhibiting apoptosis. The image was created with Figdraw (www.figdraw.com). G-Rb_3, ginsenoside Rb_3; OGD/R, oxygen-glucose deprivation/reoxygenation.

phosphoglycolic acid, guanosine and suberic acid. The screening results are presented in Table SII.

Differential metabolite analysis. Heatmaps provide relative quantitative hierarchical clustering of differential metabolites, where clustered metabolites have similar expression patterns and may have similar functions or participate in the same metabolic processes or cellular pathways. Red color indicates the higher expression level and blue colour indicates lower expression level (Fig. 3G). The distribution of differential metabolites between the two groups of samples can be visualized using a volcano plot, where the horizontal coordinates represent the multiplicity of differences and the vertical coordinates represent the significance. Red represents metabolites with significant upregulation, blue represents metabolites with significant downregulation and gray represents metabolites with no significant differences (Fig. 3H). To observe the overall changes in metabolism, this assessment captured the average and overall changes in all metabolites in the pathway based on differential abundance scores. The differential metabolites between the G-Rb_3 and OGD/R groups mainly interacted through ABC transporters, galactose metabolism, glyoxylate and dicarboxylate metabolism, citrate cycle, linoleic acid metabolism and other different pathways affect nerves, energy metabolism and other systems together. These data illustrated that the higher the contribution of a detected metabolite under the ABC transporters and galactose metabolism pathways, the more significant is the effect of the differential metabolite on these pathways (Fig. 3I).

Apoptosis PCR array. A total of 87 target genes in the apoptosis PCR array (Fig. 4A) were investigated, according to the '$\log_2$FoldChange' value as a reference. In total, the results revealed that 30 target genes were upregulated and 57 target genes were downregulated (Table SIII). The differential genes screened according to $|\log_2 \text{FoldChange}| \geq 1$ were the following: *Trp63*, *Trp73*, *Dapk1*, *Casp14* and *Cd70*, all of which were downregulated in expression by the action of G-Rb_3 (Fig. 4B).

Discussion

In the present study, hippocampal neuron HT22 cells were used to replicate the OGD/R model for simulation of CIRI, and to explore the mechanism of G-Rb_3 against OGD/R injury in apoptosis at the metabolite level. Under normal conditions, Bcl-2 family member Bax exists in the cytoplasm as a monomer. Apoptosis is caused by the interaction between pro- and anti-apoptotic members of the Bcl-2 family, which activates the release of the hydrolase caspase-3 into the cytoplasm. This in turn activates the form of caspase-3 which can damage the cytoskeleton and organelles, and degrade DNA and other proteins (28,29). Following intervention with G-Rb_3, the expression between Bax and Bcl-2 is balanced and inhibited, thereby protecting HT22 cells from damage caused by CIRI. Apoptosis is the most important determinant of stroke, and inhibiting apoptosis is a key treatment factor (30,31). Although preliminary studies by the group have shown that G-Rb_3 may reduce the damage caused by OGD/R through

antioxidant effect, the mechanism of action at the metabolite level remains unclear. Therefore, based on the authors' research group, cell viability was detected by trypan blue staining and cell apoptosis was assessed with flow cytometry. The Bax and Bcl-2 proteins play a key regulatory role in the process of apoptosis. Specifically, the ischemic stroke stimulates Bax translocation, triggering apoptosis, which Bcl-2 acts to prevent. Therefore, the ratio of Bax to Bcl-2 has an important role in apoptosis (32,33). Caspase-3 is an enzyme that promotes apoptotic proteins, playing a key regulatory role in a variety of apoptotic pathways and leading to apoptosis due to cleavage when apoptotic signals are received (34,35). In the present study, WB assays were conducted to show that G-Rb_3 increased the expression of anti-apoptotic protein Bcl-2, and decreased that of pro-apoptotic protein Bax and caspase-3 protein. Taken together, these results demonstrated that G-Rb_3 alleviated OGD/R injury by inhibiting apoptosis.

Starting at the metabolite level in the exploration of the mechanism of action of G-Rb_3, it was revealed that its protective effect on OGD/R-induced HT22 cells was mainly mediated through changes in metabolites such as nitrogen-containing organic compounds and lipid compounds. A total of 31 metabolites were analyzed for between-group differences between the G-Rb_3 and OGD/R groups. A total of 12 metabolites were upregulated after G-Rb_3 intervention, such as 3-indolacetonitrile, enalaprilat, (R) 2,3-dihydroxy-3-methylvalerate, sorbitol, 4-pyridoxic acid, 4-fumarylacetoacetate and pimelic acid. On the other hand, a total of 19 metabolites were downregulated, such as D-arabitol, D-lyxose, cis-aconitate, 6-phosphogluconic acid, isocitric acid, adipic acid and guanosine. One of these metabolites, guanosine, belongs to the group of endogenous guanine nucleosides that have been shown to protect neurons from damage and induced cell death; it as a trophic factor to promote neuroprotection during oxygen-glucose deprivation, and to exert anti-inflammatory effects (36-38). D-galactose is a naturally occurring aldose in the body, which is usually metabolized into glucose by galactokinase and uridine transferase, and stored as glycogen in liver, muscle and adipose tissue. When administered at high doses, exogenous D-galactose induces senescent effects in several organs by increasing oxidative stress, apoptosis and inflammation. This in turn leads to cognitive decline; however, ameliorating oxidative stress in hippocampal neurons can alleviate such damage. *In vitro* assays revealed that D-galactose decreases the viability of HT22 cells and causes apoptosis (39-41). Yohimbine is a selective α_2-adrenergic blocking agent with neuroprotective effect (42). Sorbitol is an osmotic dehydrating diuretic drug that acts, by increasing plasma osmolality, drawing water out of the eye, brain and othertissues into the blood vessels, reducing tissue edema, protecting brain tissue and indirectly protecting HT22 cells (43). Previous studies have shown a close relationship between stroke and high blood pressure (44-46). Hypertension causes >1.5 million strokes each year and the second highest number of deaths worldwide. Antihypertensive therapy helps to prevent most ischemic strokes. Enalaprilat belongs to the angiotensin-converting enzyme inhibitors drug class, which significantly reduces systolic and diastolic blood pressure. The drugs normalize central and cerebral hemodynamic parameters and reduce the degree of strain on the renin-angiotensin-aldosterone regulatory system, thus protecting stroke patients and indirectly protecting HT22 cell damage (44-46). Linoleic acid protects OGD/R damage by inhibiting the increase of Ca^{2+} induced by OGD, causing an increase in reactive oxygen species levels and reducing apoptosis (47). The aforementioned metabolites that were altered after G-Rb_3 intervention are closely related to apoptosis. Therefore, it was hypothesized that increases or decreases in the levels of these metabolites might be related to G-Rb_3 mediated protection against OGD/R induced HT22 cell damage through inhibition of apoptosis. Subsequent KEGG enrichment analysis demonstrated that G-Rb_3 might act by regulating metabolic pathways involving ABC transporters, galactose metabolism and citrate cycle. This led to the hypothesis that guanosine may have potential as a biomarker for the diagnosis of CIRI attenuated by G-Rb_3.

Based on the metabolomics-based analysis, the expression of apoptotic genes using PCR array with $|\log_2 FC| \geq 1$ was verified as the screening condition. This identified the following five differential genes, all of which are pro-apoptotic: i) *Trp63* and *Trp73*, the main members of the *Trp53* family, which induce apoptosis when they are overexpressed (48,49); ii) *Dapk1*, the key gene in the process of ischemic neuronal death (50); iii) *Casp14*, a member of the caspase family and a central player in the execution phase of apoptosis (51); and iv) *Cd70*, which belongs to the tumour necrosis factor family and induces apoptosis by regulating T-cell activity (52-54). The results of the present study showed that G-Rb_3 significantly downregulated these five pro-apoptotic genes, with consistent results in PCR array and WB assays. Combined with the flow cytometry and trypan blue staining results, the data consistently support a possible role for G-Rb_3 in the inhibition apoptosis.

Owing to the relative complexity of the pathogenesis of stroke, there are certain limitations to the present study, such as the lack of verification of metabolites and metabolic pathways and the research angle being relatively simple. In addition, it was not verified whether other active components of *Panax notoginseng* have a protective effect on cerebral ischemia and reperfusion. The lack of in-depth analysis affects the comprehensiveness of the research results. Validation of metabolomics results by animal experiments will be considered.

In conclusion, it was found in the present study that G-Rb_3 protects against OGD/R injury through a mechanism involving altered guanosine and regulation of the ABC transporters metabolic pathway to inhibit apoptosis (Fig. 5). It can be hypothesized that G-Rb_3 can improve CIRI. While there remain numerous other complex pathological factors of stroke to be examined in the future, the present study provides a reference for the clinical application of G-Rb_3 in the treatment of stroke.

Acknowledgements

Not applicable.

Funding

The present study was supported by the Regularity and Mechanism of Prescriptions Containing *Panax notoginseng* based on Data Mining and Network Pharmacology (grant no. 2022J0953).

Availability of data and materials

The data generated in the present study may be requested from the corresponding author. The metabolomics data that have been generated in the present study may be found in the EMBL-EBI MetaboLights database under accession number MTBLS10570 or at the following URL: https://www.ebi.ac.uk/metabolights/MTBLS10570.

Authors' contributions

FL was the main contributor to the present study to formulate the experimental scheme. JT and XD designed the experiments and performed data analysis. MZ and JT conducted the statistical analysis and confirm the authenticity of all the raw data. XY and TX examined the relevant indicators of the experiment and contributed to statistical analysis of the data. CW interpreted the research results and modified the manuscript. All authors read and approved the final version of the manuscript.

Ethics approval and consent to participate

Not applicable.

Patient consent for publication

Not applicable.

Competing interests

The authors declare that they have no competing interests.

References

1. Markus HS: Stroke genetics. Hum Mol Genet 20: R124-R131, 2011.
2. Abbas M, Malicke DT and Schramski JT: Stroke anticoagulation. In: StatPearls. StatPearls Publishing, Treasure Island, FL, 2024.
3. Campbell BCV and Khatri P: Stroke. Lancet 396: 129-142, 2020.
4. Campbell BCV, De Silva DA, Macleod MR, Coutts SB, Schwamm LH, Davis SM and Donnan GA: Ischaemic stroke. Nat Rev Dis Primers 5: 70, 2019.
5. Xu C, Wang W, Wang B, Zhang T, Cui X, Pu Y and Li N: Analytical methods and biological activities of *Panax notoginseng* saponins: Recent trends. J Ethnopharmacol 236: 443-465, 2019.
6. Liang Z, Liu K, Li R, Ma B, Zheng W, Yang S, Zhang G, Zhao Y, Chen J and Zhao M: An instant beverage rich in nutrients and secondary metabolites manufactured from stems and leaves of *Panax notoginseng*. Front Nutr 9: 1058639, 2022.
7. Chen XM, Chen HS, Xu MJ and Shen JG: Targeting reactive nitrogen species: a promising therapeutic strategy for cerebral ischemia-reperfusion injury. Acta pharmacologica Sin 34: 67-77, 2013.
8. Thorén M, Dixit A, Escudero-Martínez I, Gdovinová Z, Klecka L, Rand VM, Toni D, Vilionskis A, Wahlgren N and Ahmed N: Effect of recanalization on cerebral edema in ischemic stroke treated with thrombolysis and/or endovascular therapy. Stroke 51: 216-223, 2020.
9. Takahashi H, Yamamoto T and Tsuboi A: Molecular mechanisms underlying activity-dependent ischemic tolerance in the brain. Neurosci Res 186: 3-9, 2023.
10. Zheng MM, Zhang F and Zhang Q: Research progress in biological activity of ginsenoside Rb3. Central South Pharm 9: 1249-1252, 2017 (In Chinese).
11. Liu X, Jiang Y, Yu X, Fu W, Zhang H and Sui D: Ginsenoside-Rb3 protects the myocardium from ischemia-reperfusion injury via the inhibition of apoptosis in rats. Exp Ther Med 8: 1751-1756, 2014.
12. Kim DH, Kim DW, Jung BH, Lee JH, Lee H, Hwang GS, Kang KS and Lee JW: Ginsenoside Rb2 suppresses the glutamate-mediated oxidative stress and neuronal cell death in HT22 cells. J Ginseng Res 43: 326-334, 2019.
13. Qian T, Cai Z, Wong RNS, Mak NK and Jiang ZH: In vivo rat metabolism and pharmacokinetic studies of ginsenoside Rg3. J Chromatogr B Analyt Technol Biomed Life Sci 816: 223-232, 2005.
14. Qian T, Cai Z, Wong RNS and Jiang ZH: Liquid chromatography/mass spectrometric analysis of rat samples for in vivo metabolism and pharmacokinetic studies of ginsenoside Rh2. Rapid Commun Mass Spectrom 19: 3549-3554, 2005.
15. Zhou S, Gao X, Chen C, Zhang J, Zhang Y, Zhang L and Yan X: Porcine cardiac blood-Salvia miltiorrhiza root alleviates cerebral ischemia reperfusion injury by inhibiting oxidative stress induced apoptosis through PI3K/AKT/Bcl-2/Bax signaling pathway. J Ethnopharmacol 316: 116698, 2023.
16. Yuan Y, Tian Y, Jiang H, Cai LY, Song J, Peng R and Zhang XM: Mechanism of PGC-1α-mediated mitochondrial biogenesis in cerebral ischemia-reperfusion injury. Front Mol Neurosci 16: 1224964, 2023.
17. Schrimpe-Rutledge AC, Codreanu SG, Sherrod SD and McLean JA: Untargeted metabolomics strategies-challenges and emerging directions. J Am Soc Mass Spectrom 27: 1897-1905, 2016.
18. Wishart DS: Metabolomics for investigating physiological and pathophysiological processes. Physiol Rev 99: 1819-1875, 2019.
19. Smith CA, Want EJ, O'Maille G, Abagyan R and Siuzdak G: XCMS: Processing mass spectrometry data for metabolite profiling using nonlinear peak alignment, matching, and identification. Anal Chem 78: 779-787, 2006.
20. Navarro-Reig M, Jaumot J, García-Reiriz A and Tauler R: Evaluation of changes induced in rice metabolome by Cd and Cu exposure using LC-MS with XCMS and MCR-ALS data analysis strategies. Anal Bioanal Chem 407: 8835-8847, 2015.
21. Cheng J, Li G, Yang L, Chen P and Duan X: Alcohol extract of Rubia yunnanensis: Metabolic alterations and preventive effects against OGD/R-induced oxidative damage in HT22 cells. Biomed Rep 20: 75, 2024.
22. Wishart DS, Tzur D, Knox C, Eisner R, Guo AC, Young N, Cheng D, Jewell K, Arndt D, Sawhney S, *et al*: HMDB: The human metabolome database. Nucleic Acids Res 35 (Database Issue): D521-D526, 2007.
23. Horai H, Arita M, Kanaya S, Nihei Y, Ikeda T, Suwa K, Ojima Y, Tanaka K, Tanaka S, Aoshima K, *et al*: MassBank: A public repository for sharing mass spectral data for life sciences. J Mass Spectrom 45: 703-714, 2010.
24. Sud M, Fahy E, Cotter D, Brown A, Dennis EA, Glass CK, Merrill AH Jr, Murphy RC, Raetz CR, Russell DW and Subramaniam S: LMSD: LIPID MAPS structure database. Nucleic Acids Res 35 (Database Issue): D527-D532, 2007.
25. Abdelrazig S, Safo L, Rance GA, Fay MW, Theodosiou E, Topham PD, Kim DH and Fernández-Castané A: Metabolic characterisation of Magnetospirillum gryphiswaldense MSR-1 using LC-MS-based metabolite profiling. RSC Adv 10: 32548-32560, 2020.
26. Kanehisa M and Goto S: KEGG: Kyoto encyclopedia of genes and genomes. Nucleic Acids Res 28: 27-30, 2000.
27. Xia J and Wishart DS: Web-based inference of biological patterns, functions and pathways from metabolomic data using MetaboAnalyst. Nat Protoc 6: 743-760, 2011.
28. Barman J, Kumar R, Saha G, Tiwari K and Dubey VK: Apoptosis: Mediator molecules, interplay with other cell death processes and therapeutic potentials. Curr Pharm Biotechnol 19: 644-663, 2018.
29. Flores-Romero H, Ros U and Garcia-Saez AJ: Pore formation in regulated cell death. EMBO J 39: e105753, 2020.
30. Yuan J, Zeng L, Sun Y, Wang N, Sun Q, Cheng Z and Wang Y: SH2B1 protects against OGD/R-induced apoptosis in PC12 cells via activation of the JAK2/STAT3 signaling pathway. Mol Med Rep 18: 2613-2620, 2018.
31. Peña-Blanco A and García-Sáez AJ: Bax, Bak and beyond-mitochondrial performance in apoptosis. FEBS J 285: 416-431, 2018.
32. Brady HJ and Gil-Gómez G: Bax. The pro-apoptotic Bcl-2 family member, Bax. Int J Biochem Cell Biol 30: 647-650, 1998.
33. Edlich F: BCL-2 proteins and apoptosis: Recent insights and unknowns. Biochem Biophys Res Commun 500: 26-34, 2018.
34. Trubiani O, Guarnieri S, Paganelli R and Di Primio R: Involvement of caspace-3 in the cleavage of terminal transferase. Int J Immunopathol Pharmacol 15: 201-208, 2002.

35. Dal-Cim T, Ludka FK, Martins WC, Reginato C, Parada E, Egea J, López MG and Tasca CI: Guanosine controls inflammatory pathways to afford neuroprotection of hippocampal slices under oxygen and glucose deprivation conditions. J Neurochem 126: 437-450, 2013.
36. Rathbone M, Pilutti L, Caciagli F and Jiang S: Neurotrophic effects of extracellular guanosine. Nucleosides Nucleotides Nucleic Acids 27: 666-672, 2008.
37. Oliveira KA, Dal-Cim TA, Lopes FG, Nedel CB and Tasca CI: Guanosine promotes cytotoxicity via adenosine receptors and induces apoptosis in temozolomide-treated A172 glioma cells. Purinergic Signal 13: 305-318, 2017.
38. Schneider EH, Hofmeister O, Kälble S and Seifert R: Apoptotic and anti-proliferative effect of guanosine and guanosine derivatives in HuT-78 T lymphoma cells. Naunyn Schmiedebergs Arch Pharmacol 393: 1251-1267, 2020.
39. Shwe T, Pratchayasakul W, Chattipakorn N and Chattipakorn SC: Role of D-galactose-induced brain aging and its potential used for therapeutic interventions. Exp Gerontol 101: 13-36, 2018.
40. Xue A, Zhao D, Zhao C, Li X, Yang M, Zhao H, Zhao C, Lei X, Wu J and Zhang N: Study on the neuroprotective effect of Zhimu-Huangbo extract on mitochondrial dysfunction in HT22 cells induced by D-galactose by promoting mitochondrial autophagy. J Ethnopharmacol 318: 117012, 2024.
41. Kwon HJ, Hahn KR, Nam SM, Yoon YS, Moon SM, Hwang IK, and Kim DW: Purpurin ameliorates D-galactose-induced aging phenotypes in mouse hippocampus by reducing inflammatory responses. Neurochem Int 167: 105552, 2023.
42. Jabir NR, Firoz CK, Zughaibi TA, Alsaadi MA, Abuzenadah AM, Al-Asmari AI, Alsaieedi A, Ahmed BA, Ramu AK and Tabrez S: A literature perspective on the pharmacological applications of yohimbine. Ann Med 54: 2861-2875, 2022.
43. Bremer AM, Yamada K and West CR: Ischemic cerebral edema in primates: effects of acetazolamide, phenytoin, sorbitol, dexamethasone, and methylprednisolone on brain water and electrolytes. Neurosurgery 6: 149-154, 1980.
44. Mailloux A, Deslandes B, Vaubourdolle M and Baudin B: Captopril and enalaprilat decrease antioxidant defences in human endothelial cells and are unable to protect against apoptosis. Cell Biol Int 27: 825-830, 2003.
45. Gomez HJ, Cirillo VJ and Irvin JD: Enalapril: A review of human pharmacology. Drugs 30 (Suppl 1): S13-S24, 1985.
46. Niu JJ, Bai Lf and Hou CN: Comparison of therapeutic effects of captopril, enalapril and sodium nitroprusside on hypertension, 2018.
47. Turovsky EA, Varlamova EG, Gudkov SV and Plotnikov EY: The protective mechanism of deuterated linoleic acid involves the activation of the $Ca2^{+}$ signaling system of astrocytes in ischemia in vitro. Int J Mol Sci 22: 13216, 2021.
48. Kenzelmann Broz D and Attardi LD: TRP53 activates a global autophagy program to promote tumor suppression. Autophagy 9: 1440-1442, 2013.
49. Jacobs WB, Govoni G, Ho D, Atwal JK, Barnabe-Heider F, Keyes WM, Mills AA, Miller FD and Kaplan DR: p63 is an essential proapoptotic protein during neural development. Neuron 48: 743-756, 2005.
50. Wei R, Zhang L, Hu W, Wu J and Zhang W: Long non-coding RNA AK038897 aggravates cerebral ischemia/reperfusion injury via acting as a ceRNA for miR-26a-5p to target DAPK1. Exp Neurol 314: 100-110, 2019.
51. Markiewicz A, Sigorski D, Markiewicz M, Owczarczyk-Saczonek A and Placek W: Caspase-14-from biomolecular basics to clinical approach. A review of available data. Int J Mol Sci 22: 5575, 2021.
52. Hoefsmit EP, van Royen PT, Rao D, Stunnenberg JA, Dimitriadis P, Lieftink C, Morris B, Rozeman EA, Reijers ILM, Lacroix R, *et al*: Inhibitor of apoptosis proteins antagonist induces T-cell Proliferation after cross-presentation by dendritic cells. Cancer Immunol Res 11: 450-465, 2023.
53. Sasnauskiene A, Kadziauskas J, Vezelyte N, Jonusiene V and Kirveliene V: Apoptosis, autophagy and cell cycle arrest following photodamage to mitochondrial interior. Apoptosis 14: 276-286, 2009.
54. Wensveen FM, Unger PPA, Kragten NAM, Derks IA, ten Brinke A, Arens R, van Lier RA, Eldering E and van Gisbergen KP: CD70-driven costimulation induces survival or Fas-mediated apoptosis of T cells depending on antigenic load. J Immunol 188: 4256-4267, 2012.